Condensed Matter Physics, 2004, Vol. 7, No. 2(38), pp. 247–264

CONDENSED MATTER PHYSICS

Density-functional calculations for Ce, Th, and Pu metals and alloys

A.Landa, P.Söderlind

Lawrence Livermore National Laboratory, University of California, P.O. Box 808, Livermore, CA 94550

Received April 5, 2004

The phase diagrams of Ce, Th, and Pu metals have been studied by means of density-functional theory (DFT). In addition to these metals, the phase stability of Ce-Th and Pu-Am alloys has been also investigated from first-principles calculations. Equation-of-state (EOS) for Ce, Th, and the Ce-Th alloys has been calculated up to 1 Mbar pressure in good comparison to experimental data. Present calculations show that the Ce-Th alloys adopt a body-centered-tetragonal (bct) structure upon hydrostatic compression which is in excellent agreement with measurements. The ambient pressure phase diagram of Pu is shown to be very poorly described by traditional DFT but rather well modelled when including magnetic interactions. In particular, the anomalous δ phase of Pu is shown to be stabilized by magnetic disorder at elevated temperatures. The Pu-Am system has also been studied in a similar fashion and it is shown that this system, for about 25% Am content, becomes antiferromagnetic below about 400 K which corroborates the recent discovery of a Curie-Weiss behavior in this system.

Key words: *Cerium, Thorium, Plutonium, phase diagram*

PACS: *64.10.+h, 71.15.Mb, 71.27.+a, 75.10.Lp*

1. Introduction

Actinide physics has seen a remarkable focus the last decade or so due to the combination of new experimental diamond-anvil-cell techniques and the development of fast computers and more advanced theory. All f-electron systems are expected to have multi-phase phase diagrams due to the sensitivity of the f-electron band to external influences such as pressure and temperature. For instance, compression of an f-electron metal generally causes the occupation of the f states to change due to a shift of these bands relative to others. This can, in some cases, such as in the Ce-Th systems, [1,2] cause the crystal to adopt a lower symmetry crystal structure at elevated pressures. Under compression, the f-electron dominance increases in these systems and drives the phase transition. The reason for this has been discussed [3] in terms of a Peierls or Jahn-Teller distortion that favors low symmetry

over high symmetry crystal structures. On the other hand, all bands broaden under compression and the distortion of the lattice becomes less important, while electrostatic forces tend to move atoms to higher symmetry positions, ultimately leading to closer packed structures with higher symmetry. This interplay between competing effects and their pressure dependence often results in interesting multi-phase phase diagrams and this is the case for Ce, Th, Pu, and their corresponding alloys.

The first part of our manuscript is devoted to the study of phase stabilities of Ce, Th, and Ce-Th system as a function of compression. Cerium metal has a very interesting phase diagram with two isostructural, face-centered-cubic (fcc) phases, namely the γ and α phase. The latter is considerably denser than the former and there is a substantial volume collapse associated with the $\gamma \rightarrow \alpha$ transition that occurs at a moderate pressure close to 10 kbar. The nature of this transition is currently not fully understood, but it can be described [4] as a Mott transition of the f electron from a localized (γ-Ce) to an itinerant (α-Ce) state. Below 100 kbar there is also a phase transition to a lower symmetry phase which is believed to be either orthorhombic or body-centered monoclinic [5]. Above 120 kbar, however, Ce is stabilized in a bct structure and remains in this phase up to the highest measured pressure. In this regard, Th is similar to Ce but has a simpler phase diagram. Only one phase transition has been seen at low temperatures: fcc $\rightarrow$ bct at about 600 kbar. At Mbar pressures, both these metals remain in a bct crystal [6,7] with a c/a axial ratio close to 1.65. Also, the Ce-Th alloys show a similar behavior [1]. Theoretically, the Ce-Th alloys are rather well described within a density-functional approach, [2,8] although a proper, disordered, alloy treatment of the Ce-Th system has not yet been presented. In fact, it was argued that the disorder in the realistic Ce-Th alloys could not be well modelled by an ordered compound. The theoretical low pressure behavior of Ce_cTh_{1-c} was therefore erroneous [2] for $c = 0.43$. In section 3 we revisit this problem by applying a more sophisticated theory, based on the coherent potential approximation (CPA) for alloys.

Even though the Ce-Th system is well described by traditional DFT, Ce metal at low pressures seems to be affected by electron-correlations that are generally not included in the DFT. Phase stability of Th and subsequent actinides up to Pu, however, are accurately predicted by density-functional theory [9,10]. Plutonium precedes Am, which has an atomic density, crystal, and electronic structure much different from that of Pu. These differences are attributed to the localization of $5f$ electrons that occurs between Pu and Am. Many facets of Pu actually suggest that this localization has already begun in Pu. For instance, some phases in the Pu phase diagram share properties with Am. δ-Pu, which is stable at 593 K, is fcc with an atomic volume 25% greater than the monoclinic ground-state α phase. The fcc crystal structure is close-packed and quite similar to the double-hexagonal close-packed (dhcp) of Am. Also, the δ-Pu atomic density is much closer to Am than that of the ground-state α phase. Hence, there are dramatic changes with temperature in the Pu electronic structure and these cannot be understood from the traditional DFT that is generally used for the light actinides [9]. This problem was early recognized and during the last few years new models and various corrections

to the DFT have been proposed to mainly deal with δ-Pu. A description of these attempts was recently given [11]. Perhaps the most natural procedure is to consider magnetic interactions that have often been ignored in the past for plutonium because of the belief that these are of negligible importance. Many researchers have now, however, concluded that magnetic effects are necessary to include in any model for δ-Pu and δ-stabilized alloys of Pu. In section 4 we will review some recent results for Pu including energetics of the ambient pressure phase diagram and the stability of δ-Pu. The theory is expanded in section 5 to also include results for the δ-Pu-Am system.

The paper is organized as follows. Our computational approach is discussed in section 2, followed by results from the Ce-Th (section 3), Pu (section 4), and Pu-Am (section 5) calculations. We present our conclusions in the last section 6.

2. Computational details

The calculations we have referred to as exact muffin-tin orbitals (EMTO) are performed using scalar-relativistic, spin-polarized Green's function technique based on an improved screened Korringa-Kohn-Rostoker (KKR) method, where the one-electron potential is represented by optimized overlapping muffin-tin (OOMT) potential spheres [12–15]. Inside the potential spheres the potential is spherically symmetric and it is constant between the spheres. The radii of the potential spheres, the spherical potentials inside the spheres, and the constant value from the interstitial are determined by minimizing (a) the deviation between the exact and overlapping potentials and (b) the errors coming from the overlap between spheres. Thus, the OOMT potential ensures a more accurate description of the full potential compared to the conventional muffin-tin or non-overlapping approach.

Within the EMTO formalism, the one-electron states are calculated *exactly* for the OOMT potentials. As an output of the EMTO calculations, one can determine the self-consistent Green's function of the system and the complete, non-spherically symmetric charge density. Finally, the total energy is calculated using the full charge density technique, [15,16].

For the total energy of random substitutional alloys, the EMTO method has been recently combined with the CPA [17] that also allows for the treatment of magnetic disorder [18,19]. In the present work, as well as in our previous papers, [20–23] a paramagnetic (PM) δ-Pu was modelled within the disordered local moment (DLM) approximation [24]. In order to calculate this state, one uses a random mixture of two distinct magnetic states, namely, the spin up and spin down configurations of the same atomic species in the system.

The calculations are performed for a basis set including valence *spdf* orbitals and the semi-core $6p$ state whereas the core states were recalculated at each iteration. Integration over the irreducible wedge of the fcc Brillouin zone (BZ) is performed using the special k-point method [25]. The Green's function has been calculated for 40 complex energy points distributed exponentially on a semicircle with a 1.9 Ry diameter enclosing the occupied states.

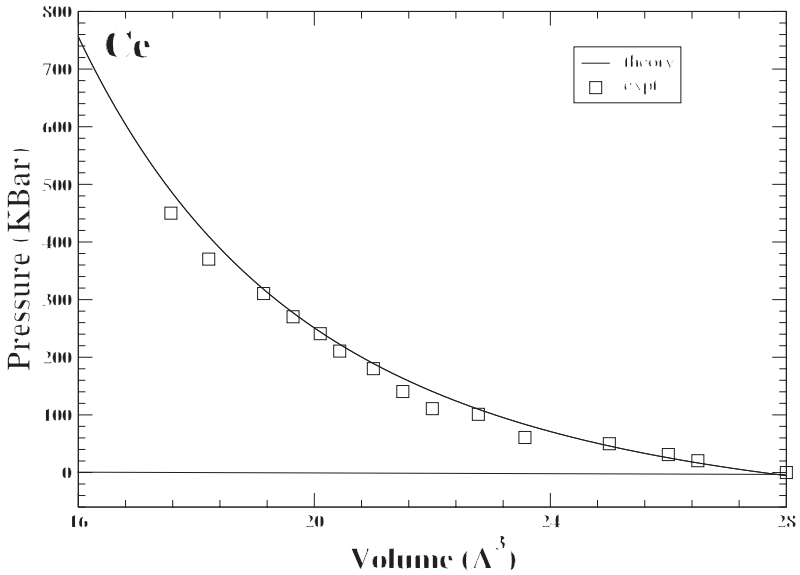

Figure 1. Equation of state for Ce. Experimental results [6] are marked with open squares, whereas theory is given by a solid line.

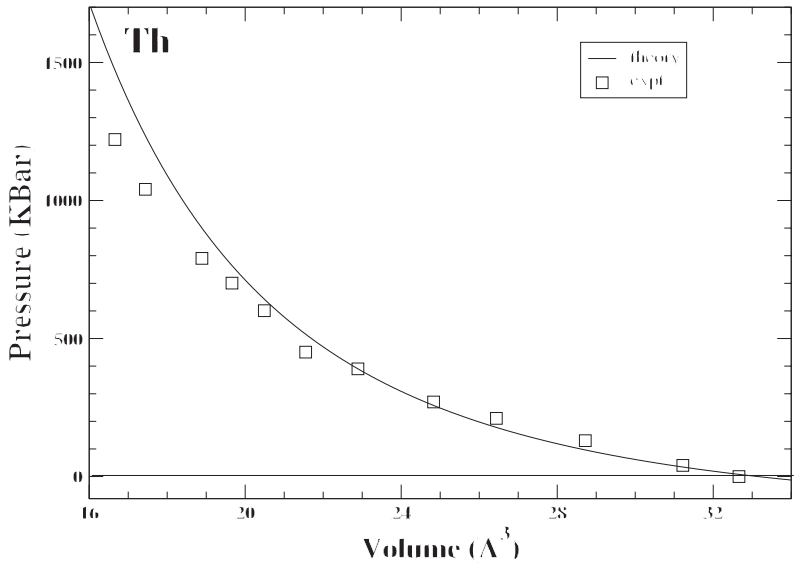

Figure 2. Equation of state for Th. Experimental results [28] are marked with open squares, whereas theory is given by a solid line.

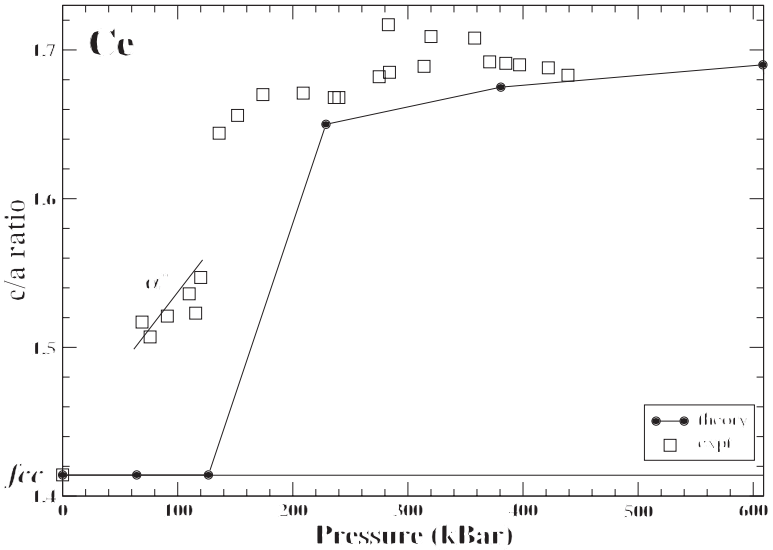

Figure 3. The c/a axial ratio for the bct structure as a function of pressure for Ce. Experimental data [6] are marked with open squares while theoretical results are given by a solid line and filled circles.

3. Ce, Th, and the Ce-Th alloys

Before entering the details of the crystal structure of Ce and Th under compression, we compare our calculated EOS with the experimental data for these two metals. In figure 1 we show the theoretical and measured equations of state for Ce metal. The agreement between theory and experiment [6] is good. Calculated equilibrium volume and bulk modulus are $V_0 = 27.7$ Å^3 and $B_0 = 380$ kbar compares well with room temperature data [26,27] ($V_0 = 28.0$ Å^3 and $B_0 = 290$ kbar). Also for Th, the EOS is in good agreement with experiment, [28] see figure 2. The Th equilibrium volume, 33.3 Å^3, and bulk modulus, 580 kbar, are very close to measured data, [28] 32.9 Å^3 and 580 kbar, respectively.

Next we study the crystal-structure behavior for Ce, and in figure 3 we plot the calculated c/a axial ratio for bct Ce together with experimental data [6]. At pressures beyond about 120 kbar, cerium adopts a bct structure with a c/a ratio close to 1.65. Quantitatively, this behavior is reproduced by our calculations. We note that there is a rapid increase of the c/a axial ratio in the calculations were there is known to be an intermediate phase [6] in Ce (below 100 kbar). The intermediate, lower symmetry phase, is limited to a small pressure range and is not considered in the present calculations, but has been investigated theoretically before [9]. A similar behavior is found for thorium metal, see figure 4. Experimentally, Th is stable in its ambient pressure phase (fcc) up to 630 kbar. At higher compression Th transforms continuously into the bct phase. The transition pressure (≈ 630 kbar) is considerably higher in Th than in Ce. The fact that the fcc $\rightarrow$ bct transition occurs at a higher pressure in Th than in Ce is a consequence of the somewhat lower f-band population in Th metal at low pressure [2].

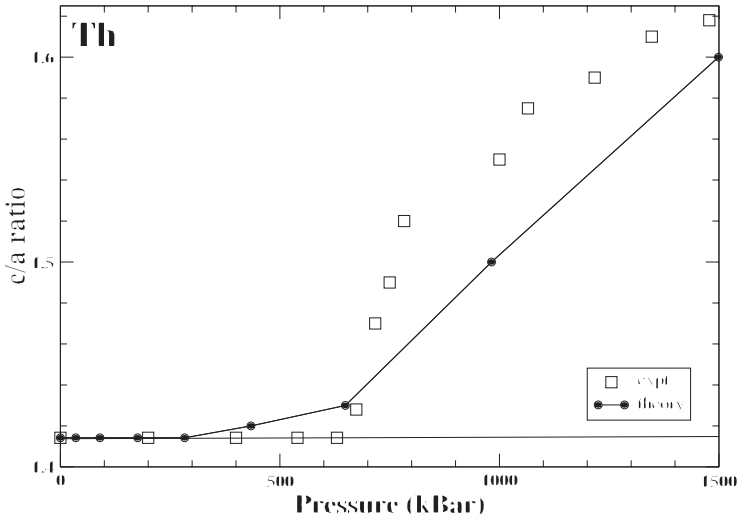

Figure 4. The c/a axial ratio for the bct structure as a function of pressure for Th. Experimental data [7] are marked with open squares while theoretical results are given by a solid line and filled circles.

As we established that elemental Ce and Th can be very well described by our calculations we next consider the $Ce_{43}Th_{57}$ disordered fcc alloy. In figure 5 we show theoretical EOS for the $Ce_{43}Th_{57}$ disordered fcc alloy. Notice that the $Ce_{43}Th_{57}$ alloy curve is located between the curves for pure Th and Ce, which are also depicted in this figure. Calculated equilibrium atomic volume and bulk modulus of the $Ce_{43}Th_{57}$ alloy are 31.4 Å^3 and 460 kbar, respectively, which is in fair agreement with experimental data of 32.9 Å^3 and 281 kbar, [1].

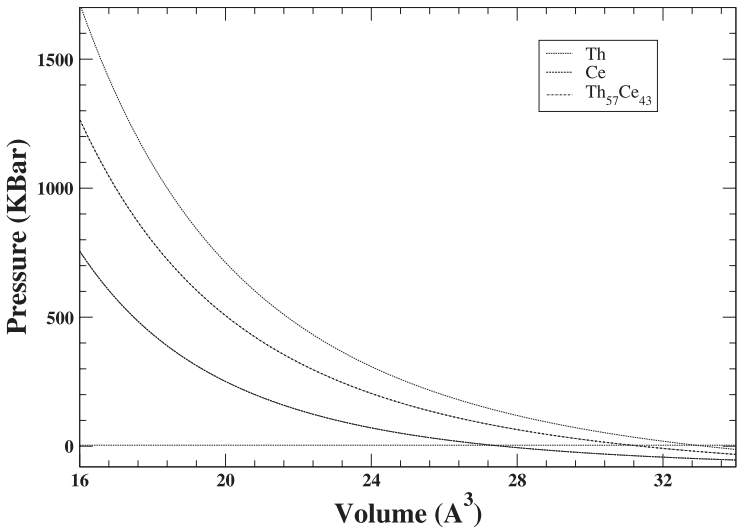

Figure 5. Equation of state for the $Ce_{43}Th_{57}$ disordered alloy. EOS for Ce and Th are also shown.

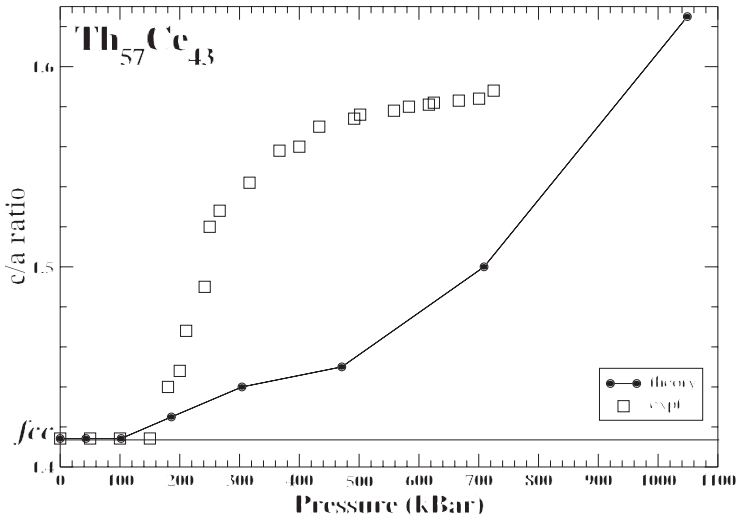

Figure 6. The c/a axial ratio for the bct structure as a function of pressure for the $Ce_{43}Th_{57}$ disordered alloy. Experimental data [1] are marked with open squares while theoretical results are given by a solid line and filled circles.

Finally, figure 6 shows the calculated and measured c/a ratio as a function of pressure for $Ce_{43}Th_{57}$. The structural behavior of this alloy was previously modelled by an ordered CeTh compound [2]. These calculations predicted unrealistic low-pressure structures for this system, where the axial c/a ratio first decreased with pressure and suddenly jumped to a high value closer to the measure value at a higher compression. It was speculated [2] that the discrepancy with experiment was due to the failure of modelling the disordered alloy with an ordered compound. Here we can address this question explicitly because the EMTO-CPA formalism allows us to treat the alloy more realistically. The EMTO-CPA calculations confirm that the fcc $\rightarrow$ bct phase transition begins between 100–200 kbar, which is close to the corresponding transition in Ce metal (120 kbar), but considerably lower than for Th (630 kbar). Our calculations thus reproduce the experimental observation [1] that the fcc $\rightarrow$ bct transition pressure is a strongly nonlinear function of Th concentration in the Ce-Th alloy system.

4. Pu metal

Pu metal and related alloys and compounds are studied intensively experimentally and theoretically, partly because of their richness of fascinating and counter intuitive properties [29]. Theoretically, the first reliable total energies for Pu were calculated not so long ago [30] and when comparing a number of competing phases, the monoclinic α phase proved to be the ground state in agreement with experiment. The α-Pu atomic volume was somewhat small and the bulk modulus too large, but a more serious deficiency of the calculations [30] seemed to be the poor description of some other phases, such as the δ phase. In figure 7 we show total energies [31] of

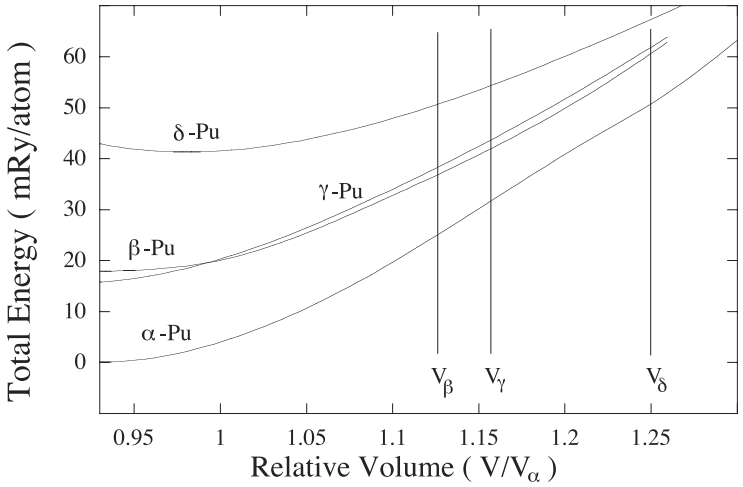

Figure 7. Total energies of α, β, γ, and δ plutonium, obtained from nonmagnetic calculations [30].

α, β, γ, and δ plutonium. Notice that β, γ, and especially δ plutonium have total energies so high that their existence in the Pu phase diagram cannot be explained. Moreover, the predicted atomic densities for these phases are close to that of α-Pu but in severe disagreement with the measured atomic volumes shown as vertical lines in figure 7. The δ phase is not even mechanically stable because the calculated elastic constant C' is strongly negative.

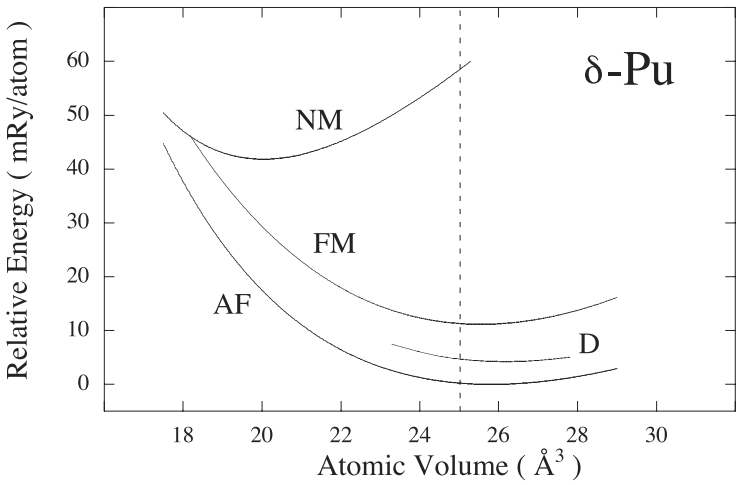

Figure 8. Total energies as a function of atomic volume for nonmagnetic (NM), ferromagnetic (FM), antiferromagnetic (AF), and disordered magnetic (D) configurations of δ-Pu [20].

The remarkable failure of the customary DFT treatment for some of the Pu phases, and most notably the δ phase, was early recognized but theoretical efforts to improve the model has only recently been suggested [31–34]. A more detailed

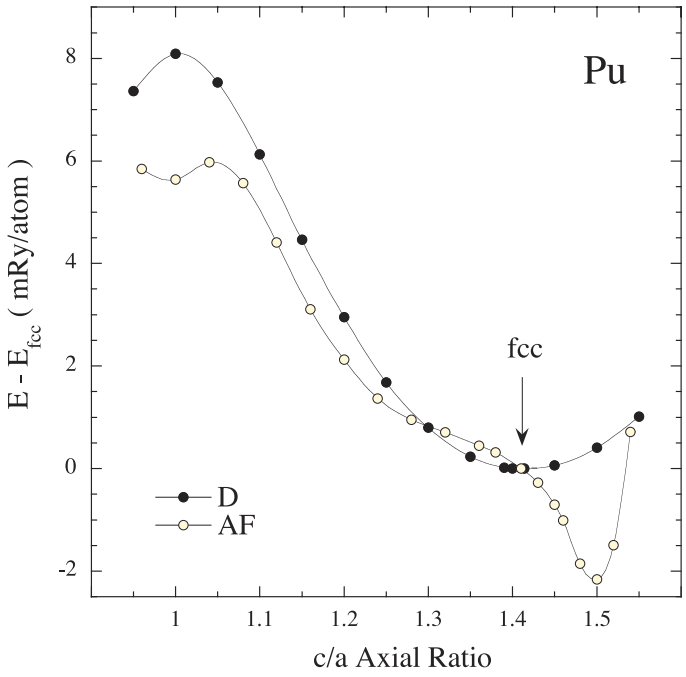

Figure 9. Total energy as a function of c/a axial ratio for antiferromagnetic (AF) and disordered magnetic (D) configurations of Pu [20].

discussion of these efforts has been presented elsewhere [11]. Because we are mainly interested in structural stability, which requires accurate and consistent total-energy calculations, most of the proposed models for Pu cannot be applied. Inclusion of magnetic interactions into the DFT, however, seems to provide a theoretical framework in which reliable total energies can be obtained [31].

Figure 8 shows total energies as a function of atomic volume for nonmagnetic (NM), ferromagnetic (FM), antiferromagnetic (AF), and disordered magnetic (D) configurations of δ-Pu [20]. Clearly, the total energies are lowered when the magnetic spin and orbital contributions are included. A direct comparison to the α phase is done below. Notice also in figure 8 that the atomic volumes for the FM, AF, and D calculations are all in good agreement with the experimental value (vertical line) while the NM calculation predicts much too small atomic volume. This plot suggests that AF is the zero temperature ground-state configuration for δ-Pu, whereas in reality this phase is stable above 593 K. The relatively small energy difference between the AF and D configurations is therefore not sufficient to rule out either one as a good model for the true δ phase. Next, we compare the mechanical stability between the AF and D δ-Pu. In figure 9 we show the calculated so-called Bain transformation path for these configurations. The energy curvature at $c/a = \sqrt{2}$ corresponds to the tetragonal shear constant C$'$. Clearly, AF spin ordering provides an unstable situation (C$'$ negative) while the magnetic disorder does not. Hence, it is tempting to suggest that spin entropy may favor the disordered state over the antiferromagnetic state at sufficiently high temperatures. If this is the case, the $\gamma \rightarrow$

δ phase transition could be understood in terms of an order $\rightarrow$ disorder transition: δ-Pu is mechanically stable in the disordered state but upon cooling a magnetic ordering destabilizes δ-Pu mechanically, thus driving the structural phase transition.

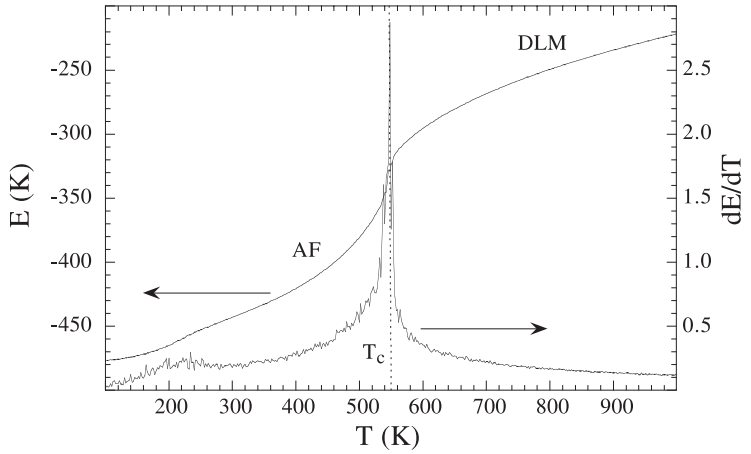

Figure 10. Total energy E and its temperature derivative dE/dT as a function of temperature in the MC simulations of δ-Pu [21].

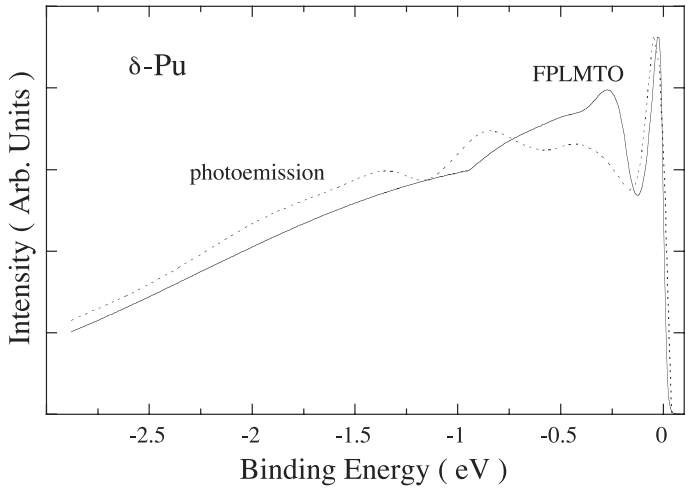

Figure 11. Comparison of spectra [35] (dashed line) to calculated DOS [20] (solid curve). The theoretical curve has been convoluted with life time broadening.

In order to quantify these ideas, Monte Carlo (MC) simulations were performed to study the transition from a disordered $\rightarrow$ ordered magnetic states of δ-Pu [21]. The effective Ising cluster interactions were obtained from first-principles calculations incorporated within the structure-inverse and general perturbation methods. Figure 10 shows the total energy per atom and its temperature derivatives in these

MC simulations. The calculated transition temperature (≈ 548 K) is in good agreement with the temperature measured at the $\gamma \rightarrow \delta$ transition of plutonium (593 K).

Once we established that a paramagnetic (disordered moments) approach provides a viable model for δ-Pu, direct comparisons with experiments become very important. First, the electronic structure has been studied [35] by means of photoemission (PE). PE is a probe of the occupied part of the electron density of states (DOS) and can be directly compared to the calculated electronic structure when lifetime broadening and instrumental resolution are accounted for. In figure 11 we show calculated DOS [20] and photoemission [35] for δ-Pu. Notice that the sharp peak just below the Fermi energy, at zero energy, is very well reproduced in the calculations. Also the shoulder, sometimes referred to as a "Kondo resonance", at about -0.3 eV is evident in the calculations although somewhat exaggerated. Overall, the comparison between theory and experiment is very impressive. It should be noted that when magnetic interactions are ignored, PE and DOS are in great disagreement with each other, [35].

Table 1. EMTO equilibrium volume (Å^3), bulk and elastic moduli (kbar), and zone-boundary phonons (THz) for δ-Pu.

Method	V	B	C′	C_{44}	X_L	X_T	L_L	L_T
EMTO	25.5	380	81	810	7.5	2.7	2.9	1.3
Experiment	25.0[1,2]	300[1], 290[2]	48[1], 49[2]	340[1], 310[2]	3.1[2]	1.7[2]	3.1[2]	0.48[2]

Recently the elastic constants and phonon dispersions for δ-stabilized plutonium were measured by x-rays [36]. The zone-boundary phonons (ZBP) are relatively straightforward to calculate from the total energy response of a movement of an atom corresponding to the phonon mode [37]. Results of EMTO calculations for ZBP and elastic constants are presented in table 1 together with available experimental data. It is clear from the table that fundamental bonding properties are captured in the calculations. Theoretical equilibrium volume as well bulk modulus compare very favorably with experiments. Also the anomalously large anisotropy ratio (C_{44}/C') is reproduced by theory. The magnitude of the calculated elastic constants and the ZBP are consistently larger than the measured data, however. We attribute this systematic discrepancy, at least partly, due to the fact that our calculations reflect these properties at zero temperature while the measurements are performed at room temperature. It is known that the elastic constants have a strong temperature dependence and stiffen considerably upon cooling [38] and it seems plausible that this is true also for the phonons. Another possible source of the discrepancy might be that the measured sample is δ-stabilized alloy whereas the theory deals with pure δ-Pu.

Our theory so far suggests that magnetic interactions are important in Pu and that δ-Pu is stabilized at 550–600 K due to magnetic disorder. Several properties of

[1]Moment R.L. [42]
[2]Wong J.*et al.* [36]

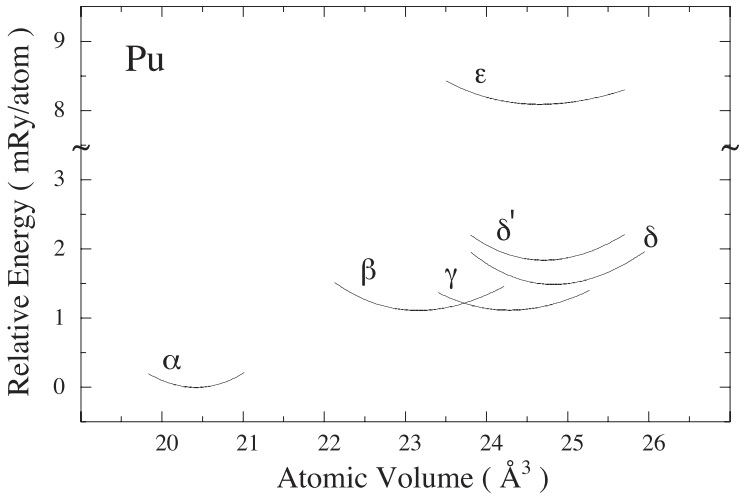

Figure 12. Calculated total energies for the six known polymorfs of plutonium as a function of atomic volume [39]. Note that the y axis is boken to better display the ϵ-Pu energies.

δ-Pu, some being quite anomalous, are indeed very well reproduced by this assumption. Higher temperature phases have presumably also disordered local magnetic moments, whereas for the lower temperature phases (α, β, and γ) the magnetic configurations are ordered. In fact, an analysis of magnetic ordering in low temperature Pu suggests antiferromagnetic order to be the prevalent configuration [39] in agreement with first-principles calculations. In figure 12 we plot calculated total energies for α, β, and γ plutonium (antiferromagnetic) together with δ, δ', and ϵ plutonium (disordered). The disordered magnetic configuration was modeled in a 8 atom super cell by the so-called special quasi-random structure [20]. Notice that the total energies are in order of α, β, γ, δ, δ', and ϵ. This is the actual order at which they do occur in the ambient pressure phase diagram [40]. The numerical order of the atomic volumes is slightly different: α, β, γ, ϵ, δ', and δ. This is again in exact agreement with the known phase diagram and that is quite remarkable when comparing to the failures of the theory when magnetic interactions are not accounted for (see figure 7). From the total energies one can obtain the bulk modulus as well, and for α-Pu it is calculated to be 500 kbar. This compares very favorably with the experimentally suggested data ranging from 400 to 660 kbar [41]. Bulk moduli for the β, γ, δ', and ϵ phases are not known, but the present theory predicts that they are all within 230–590 kbar. Notably, it is 410 kbar for δ-Pu that compares well with the measured 300–350 kbar, [42].

5. Pu-Am system

Following the idea presented in [22], we conclude that an increase of the larger element (Am) content in the Pu-Am system stabilizes the disordered magnetic state at lower temperatures. To quantify this hypothesis we undertook MC simulations

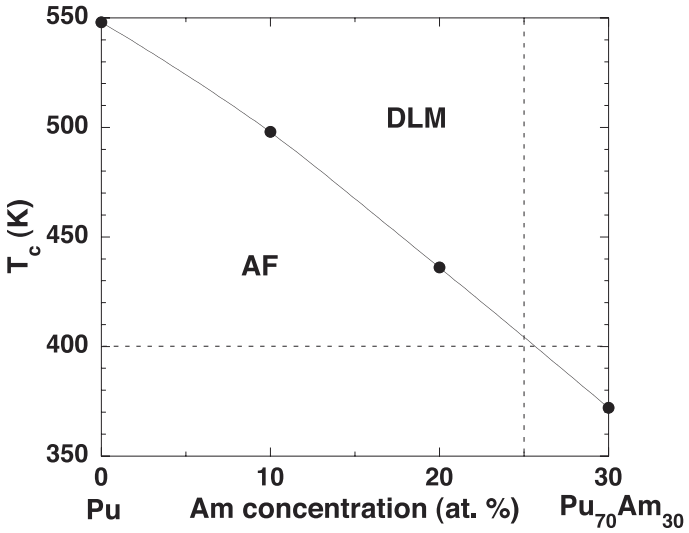

Figure 13. The DLM → AF transition temperature for $\delta-Pu_{100-c}Am_c$ alloys [23].

similar to those presented earlier [21]. Results of the MC calculations of the DLM → AF transition temperature in the Pu-Am system are shown in figure 13. By introducing Am into the Pu-Am system one could drop the magnetic DLM → AF transition temperature from ≈ 548 K (Pu) to ≈ 372 K ($Pu_{70}Am_{30}$). From the Pu-Am phase diagram, [43] however, it is known that already ≈ 6 at. % of Am could stabilize δ-Pu phase to room temperature.

As one can see from figure 13, the δ-$Pu_{75}Am_{25}$ alloy will have an AF order at and below ≈ 400 K, whereas above this temperature disordered magnetism is expected. This magnetic transition was predicted to occur also for pure δ-Pu but at a considerably higher temperature (548 K). In the case of δ-Pu the magnetic DLM → AF transition was suggested [20–22] to drive the $\delta \rightarrow \gamma$ transition due to a structural instability of the AF phase. For the Pu-Am alloy, however, no such structural phase transition has been found and this suggests that the AF configuration remains mechanically stable. Theoretically, this hypothesis can be corroborated by calculating elastic constants or relevant deformation energies for the AF Pu-Am alloy.

In figure 14 we show relative energies for AF Pu_3Am and AF δ-Pu as a function of c/a axial ratio. For $c/a = \sqrt{2}$ the fcc symmetry is recovered. Notice that for δ-Pu the AF configuration is strongly unstable with respect to the tetragonal distortion, whereas the Pu_3Am system remains mechanically stable, with a minimum in the total energy for $c/a = \sqrt{2}$. Hence, there is a fundamental difference between δ-Pu and Pu_3Am in that both undergo a magnetic DLM → AF transition that destabilizes δ-Pu but not the Pu_3Am. This is important because our theory thus predicts the possibility for an AF order in a Pu-Am alloy system. In order to verify this experimentally, one should perform magnetic susceptibility measurements that can detect a Curie-Weiss behavior when AF order is present. Dormeval [44] has performed such experiments that in fact confirm our theoretical picture. Her inves-

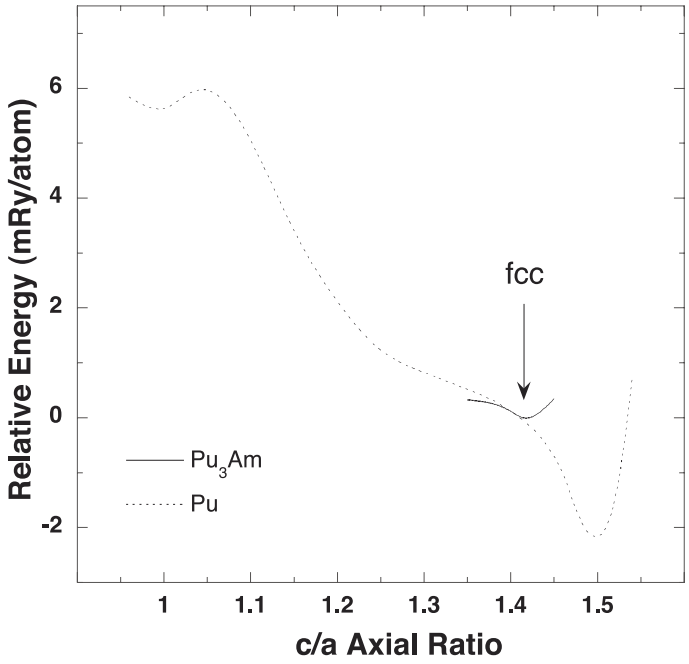

Figure 14. Relative energy as a function of c/a axial ratio for Pu and Pu_3Am [23]. For $c/a = 1.414$ the fcc crystal structure is recovered.

tigation shows that at about 24–26 at. % Am in δ-Pu, an unambiguous Curie-Weiss behavior develops. In δ-Pu, where AF order is not expected theoretically, magnetic susceptibility is known to be nearly temperature independent.

The question we deal with in the remaining part of this section is why alloying Pu with Am stabilizes the antiferromagnetic state in this alloy. Both Dormeval's measurements [44] and theoretical picture presented here support the idea that δ-Pu stabilized by ≈ 25 at. % of Am is antiferromagnetic at low temperatures. Söderlind et al., [20] however, rule out this magnetic order for pure δ-Pu due to its mechanical instability. It is well known that Pu and other actinides with itinerant $5f$ states tend to crystallize in low symmetry and open structures and that the reason for this is due to high density of $5f$ states at the Fermi level (E_F) that efficiently rules out high symmetry structures [3]. It is tempting to also associate the destabilization of antiferromagnetic δ-Pu at low temperatures to a similar phenomenon. We therefore show, in figure 15, the calculated DOS for antiferromagnetic Pu and Pu_3Am. The plot focuses on the DOS behavior in the vicinity of the E_F located at zero energy and marked with a dashed vertical line. Notice that for pure Pu, there is a strong peak intersecting the E_F with its maximum just below. This is an inherently unfavorable situation due to the large contribution of this peak to the band energy [3]. For Pu_3Am (bold line), however, this peak is shifted mostly below E_F, which is now located close to a minimum in the DOS. The DOS at the Fermi level is correspondingly much lower (≈ 25) in Pu_3Am compared to Pu (≈ 45). This shift of the E_F in Pu_3Am relative to pure Pu is a consequence of the additional $5f$ electrons provided by the americium in this compound. We speculate that this more stable situation in Pu_3Am

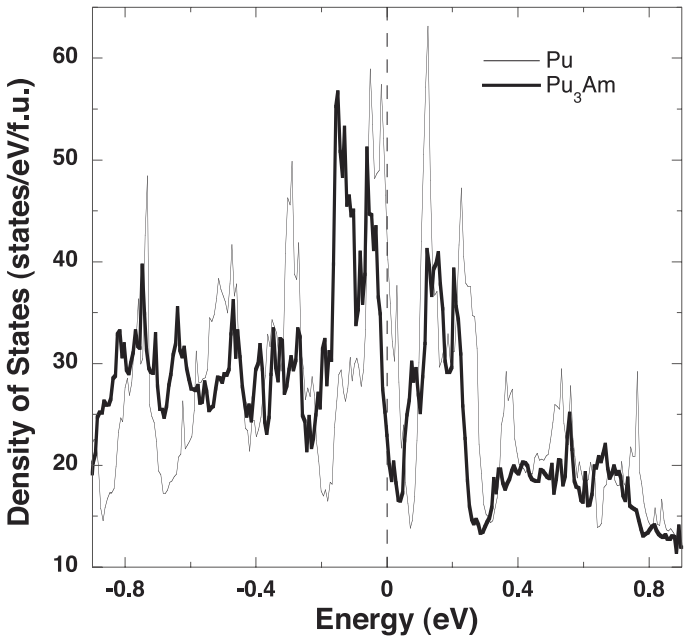

Figure 15. Lifetime broadened [35] electronic density of states for Pu and Pu_3Am [23].

is responsible for the mechanical stability in this system.

Our electronic structure calculations predict that the DOS has a pronounced peak at the E_F for Pu that is largely diminished when alloyed with about 25 at. % americium. Photoemission is capable of detecting such a difference and for that purpose we also show, in figure 16, calculated DOS where lifetime broadening has been taken into account, as described by Arko et al [35]. We know from figure 11 (section 4) that for δ-Pu the DOS compares rather well with photoemission [35] results. Figure 16 suggests that for the Pu-Am system, the peak is shifted to lower binding energies and that the shoulder at about -0.5 eV in Pu is fully suppressed. The photoelectron spectroscopy measurements by Dormeval [44] show a quantitative agreement with this finding.

6. Conclusions

We have presented accurate electronic-structure calculations for several f electron systems including Ce, Th, Pu, and Am. Generally the theory reproduces experimental data very well. The structural pressure dependence of the Ce-Th system is well understood and driven by the increased presence of f electrons under pressure. Ce, Th, and the Ce-Th alloys behave rather similar, although Ce has intermediate phases in the phase diagram at about 100 kbar that do not exist in the Th and Ce-Th alloys. Consequently, the fcc $\rightarrow$ bct transition is of first order in Ce but not in Th and the Ce-Th alloys. For the near fifty-fifty concentration of Ce-Th disordered alloy, a CPA treatment is necessary to reproduce the correct structural behavior.

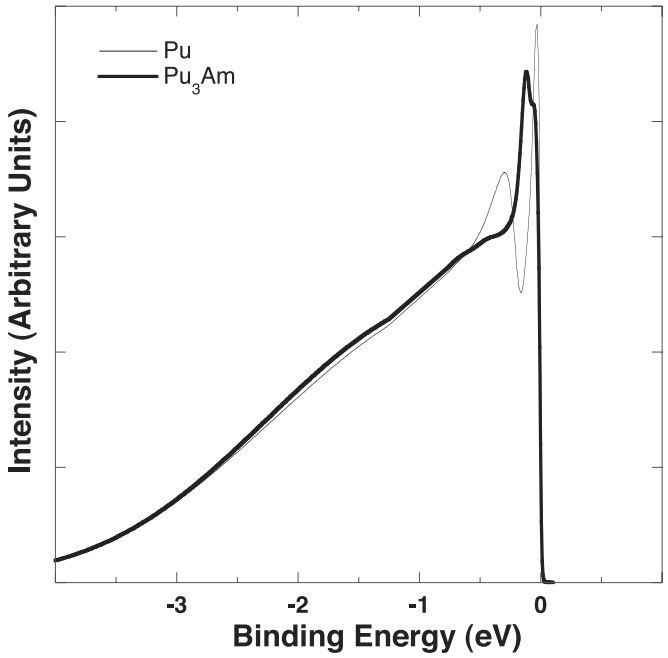

Figure 16. Total electronic density of states for Pu and Pu_3Am [23]. The energy scale is shifted so that the Fermi level is positioned at zero energy.

Many properties of Pu have not been reproduced in the past by theory and therefore been illusive to material scientists. Here we present a magnetic model that describes Pu remarkably well. The very complex phase diagram of Pu is shown to be a result of strong magnetic interactions in this metal. In particular, δ-Pu is believed to be a disordered magnet. When alloyed with Am, our theory predicts that δ-Pu is an ordered antiferromagnet above about 25% Am concentration below 400 K. This is entirely consistent with recent susceptibility measurements of this system.

7. Acknowledgments

We would like to thank Dr.A.Ruban and Dr.L.Vitos for helpful discussions. This work was performed under the auspices of the U.S. Department of Energy by the University of California Lawrence Livermore National Laboratory under contract W–7405–Eng–48.

References

1. Gu G., Vohra Y.K., Benedict U., Spirlet J.C. // Phys. Rev. B, 1994, vol. 50, p. 2751; Gu G., Vohra Y.K., Winand J.M., Spirlet J.C. // Scr. Metall. Mater, 1995, vol. 32, p. 2081.
2. Söderlind P., Eriksson O. // Phys. Rev. B, 1999, vol. 60, p. 9372.
3. Söderlind P., Eriksson O., Johansson B., Wills J.M., Boring A.M. // Nature (London), 1995, vol. 374, p. 524.

4. Johansson B., Abrikosov I.A., Alden M., Ruban A.V., Skriver H.L. // Phys. Rev. Lett., 1995, vol. 74, p. 2335.
5. McMahon M.I., Nelmes R.J. // Phys. Rev. Lett., 1998, vol. 78, p. 3884.
6. Olsen J.S., Gerward L., Benedict U., Itie J.-P. // Physica, 1985, vol. 133B, p. 129.
7. Vohra Y.K., Akella J. // Phys. Rev. Lett., 1991, vol. 67, p. 3563;
   Vohra Y.K., Akella J. // High Pres. Res., 1992, vol. 10, p. 681.
8. Söderlind P., Eriksson O., Johansson B., Wills J.M. // Phys. Rev. B, 1995, vol. 52, p. 13169.
9. Söderlind P. // Adv. Phys., 1998, vol. 47, p. 959.
10. Penicaud M. // J. of Phys.: Condens. Matter, 2000, vol 12., p. 5819.
11. Söderlind P., Landa A. // Modelling Simul. Mater. Sci. Eng., 2003, vol. 11, p. 851.
12. Andersen O.K., Jepsen O., Krier G. Methods of Electronic Structure Calculations, (eds. V. Kumar, O.K. Andersen, A. Mookerjee). Singapore, World Scientific, 1994, p. 6–124.
13. Andersen O.K., Arcangeli C., Tank R.W., Saha-Dasgupta T., G. Krier, Jepsen O., Dasgupta I. Tight-binding Approach to Computational Materials Science, (eds. Turchi P.E.A, Gonis A., Colombo L.). – In: Mater. Res. Soc. Symp. Proc. No 491 (Materials Research Society, Warrendale, 1998), p. 3–34.
14. Vitos L., Skriver H.L., Johansson B., Kollar J. // Comput. Mater. Sci., 2000. vol. 18, p. 24.
15. Vitos L. // Phys. Rev. B, 2001, vol. 64, p. 014107.
16. Kollar J., Vitos L., Skriver H.L. Electronic Structure and Physical Properties of Solids: The Uses of the LMTO Method, (ed. H. Dreysse, Lecture Notes in Physics). Berlin, Springer, 2000, p. 85–113.
17. Vitos L., Abrikosov I.A., Johansson B // Phys. Rev. Lett., 2001, vol. 87, p. 156401.
18. Landa A.I., Chang C.-C., Kumta P.N., Vitos L., Abrikosov I.A. // Solid State Ionics, 2002, vol. 149, p. 209.
19. Vitos L., Korzhavyi P.A., Johansson B. // Phys. Rev. Lett., 2002, vol. 88, p. 155501.
20. Söderlind P., Landa A., Sadigh B. // Phys. Rev. B, 2002, vol. 66, p. 205109.
21. Landa A., Söderlind P., Ruban A. // J. Phys.: Condens. Matter, 2003, vol. 15, p. L371.
22. Landa A., Söderlind P. // J. Alloys Compd., 2003, vol. 354, p. 99.
23. Landa A., Söderlind P. // J. Alloys Compd., 2004, vol. 376, (in press).
24. Györffy B.L., Pindor A.J., Stocks G.M., Staunton J., Winter H. // J. Phys. F:, 1985, vol. 15, p. 1337.
25. Chadi D.J., Cohen M.L. // Phys. Rev. B, 1973, vol. 8, p. 5747;
   Froyen S., *ibid.*, 1989, vol. 39, p. 3168.
26. Freeman A.J., Lander G.H. Handbook on the Physics and Chemistry of Actinides. Amsterdam, North-Holland, 1984, vol. 1–5.
27. Dabos S., Dufour C., Benedict U., Pages M. // J. Magn, Magn. Mater, 1987, vol. 63–64, p. 661.
28. Vohra Y.K., Holtzapfel // High Press. Res., 1993, vol. 11, p. 223.
29. Hecker S.S., Harbur D.R., Zocco T.G. // Prog. Mater. Sci., 2004, vol. 49, p. 429.
30. Söderlind P., Eriksson O., Johansson B., Wills J.M // Phys. Rev. B, 1997, vol. 55, p. 1997.
31. Söderlind P. // EuroPhys. Lett., 2001, vol. 55, p. 525.
32. Penicaud M // J. Phys.: Condens. Matter, 1997, vol. 9, p. 6341.
33. Eriksson O., Becker J.D., Balatsky A.V., Wills J.M // J. Alloys Compd., 1999, vol. 287,

p. 1.
34. Savrasov S.Y., Kotliar G., Abrahams E. // Nature, 2001, vol. 410, p. 793.
35. Arko A.J., Joyce J.J., Morales L., Wills J., Lashley J., Wastin F., Rebizant J. // Phys. Rev. B, 2000, vol. 62, p. 1773.
36. Wong J., Krisch M., Farber D.L., Occelli F., Schwartz A.J., Chiang T.-C., Wall M., Boro C., Xu R. // Science, 2003, vol. 301, p. 1078.
37. Söderlind P., Landa A., Sadigh B., Vitos L., Ruban A., (submitted to Phys. Rev. B).
38. Migliori A., Miller D.A., Lashley J.C., Freibert F., Betts J.B., Ramos M. Plutonium Futures – The Science, (ed. by Jarvinen G.D.). New York, AIP, Melville, 2003, p. 73.
39. Söderlind P., Sadigh B. // Phys. Rev. Lett., 2004, vol. 92, p. 185702.
40. Young D.A. Phase Diagrams of the Elements. Berkeley and Los Angeles, University of California Press, 1991.
41. Wick O.J. Plutonium Handbook A Guide to the Technology. New York, Gordon and Breach, 1967.
42. Moment R.L. Plutonium and Other Actinides, (ed. by Blank H. and Lindner R.). Amsterdam, North-Holland, 1976, p. 687.
43. Ellinger F.H., Johnson K.A., Struebing V.O. // J. Nucl. Mat., 1966, vol. 20, p. 83.
44. Dormeval M. Electronic Structure of Pu-Ce(-Ga) and Pu-Am(-Ga) Alloys Stabilized in the δ-Phase. Dijon, France, PhD Thesis, Universite de Bourgogne, 2001.

Розрахунки методом функціоналу густини для металів Ce, Th та Pu та сплавів

А.Ланда, П.Сюдерлінд

Лоуренс Лівермор Національна Лабораторія, Університет Каліфорнії, п.о. 808, Лівермор, CA 94550

Отримано 5 квітня 2004

Фазові діаграми металів Ce, Th та Pu вивчаються за допомогою теорії функціоналу густини (ТФГ). Крім того, фазова стабільність сплавів Ce-Th та Pu-Am досліджена з першопринципних розрахунків. Рівняння стану для Ce, Th та сплаву Ce-Th було розраховано аж до тиску 1 Мбар в доброму узгодженні з експериментальними даними. Дані розрахунки показують, що сплави Ce-Th приймають об'ємоцентровано-тетрагональну структуру внаслідок гідростатичного стиску, що чудово узгоджується з вимірюваннями. Показано, що фазова діаграма Pu при нормальному тиску дуже погано описується традиційною ТФГ, але досить добре моделюється при включенні магнітних взаємодій. Зокрема показано, що аномальна δ-фаза Pu стабілізується магнітним безладом при підвищених температурах. Система Pu-Am також була досліджена подібним чином та показано, що ця система, при приблизно 25% вмісту Am, стає антиферомагнітною нижче приблизно 400 K, що узгоджується з недавнім відкриттям поведінки Кюрі-Вейса в цій системі.

Ключові слова: *церій, торій, плутоній, фазова діаграма*

PACS: *64.10.+h, 71.15.Mb, 71.27.+a, 75.10.Lp*